Available online at www.sciencedirect.com

ScienceDirect

Procedia Computer Science 112 (2017) 1206–1215

Procedia Computer Science

www.elsevier.com/locate/procedia

International Conference on Knowledge Based and Intelligent Information and Engineering Systems, KES2017, 6-8 September 2017, Marseille, France

Numerical simulation of earthquakes impact on facilities by grid-characteristic method

Alena Favorskaya[a,b,]*, Igor Petrov[a,b], Vasiliy Golubev[a,b], Nikolay Khokhlov[a,b]

[a]*Moscow Institute of Physics and Technology, 9 Institytsky Pereylok st., Dolgoprudny, Moscow Region, 141700 Russian Federation*
[b] *Scientific Research Institute for System Studies of the Russian Academy of Sciences, 36(1) Nahimovskij av., Moscow, 117218 Russian Federation*

Abstract

Numerical modeling of dynamic wave processes in heterogeneous media allows to investigate the earthquake stability of different constructions. The aim of this work is to study the earthquakes' impact on the ground buildings and underground facilities. The use of grid-characteristic method makes possible to take into account the physics of arising wave processes. The use of systems of hierarchical grids allows to perform a calculation of seismic waves directly from the earthquake source to the ground buildings and underground facilities. The arising area of cracks in this ground building (two-storied houses) at different times from different types of seismic waves is studied. Also the impact of earthquake on the underground facilities is considered. The dynamical arising of cracks and destruction into the underground facilities made from different types of reinforced concrete due to the impact of different types of seismic waves is investigated in this paper. The results demonstrate a possibility of investigation earthquake stability of underground facilities and living buildings using modeling of seismic waves' propagation directly from the earthquake centers.

Peer-review under responsibility of KES International

*Keywords:*earthquake stability; seismic waves; hierarhical grids; wave processes; numerical modeling; grid-characteristic method

* Corresponding author. Tel.: +7-495-408-66-95; fax: +7-495-408–42–54.
E-mail address: aleanera@yandex.ru

1877-0509
Peer-review under responsibility of KES International
10.1016/j.procs.2017.08.035

1. Introduction

At the present time, the investigation of seismic stability of surface facilities is the study of great importance. The numerical simulation of seismic problems using the finite difference schemes on triangular and tetrahedral grids is discussed in researches[1-7]. Also a pseudospectral method is used to solve this class of problems[8-10] and a method of spectral elements[11-13] is applied as well. The use of grid-characteristic[14-21] method can be found in[18] in dealing with seismic problems.

In this paper, for the numerical simulation of earthquake impacts on the surface and underground facilities the grid-characteristic method on hierarchical grids was performed. The advantages of using this technique deal with the accounting of all the arising wave processes and correct statement of the boundary conditions in interface conditions. The use of hierarchical meshes makes it possible to simulate all wave processes directly from the earthquake source to the object under consideration.

2. Problem definition

The following system of equations describing the state of infinitesimal volume of continuous linear elastic medium[14-22] is solved.

$$\rho \partial_t \mathbf{v} = \left(\nabla \cdot \boldsymbol{\sigma}\right)^{\mathrm{T}} \tag{1}$$

$$\partial_t \boldsymbol{\sigma} = \rho\left(c_p^2 - 2c_s^2\right)\left(\nabla \cdot \mathbf{v}\right)\mathbf{I} + \rho c_s^2\left(\nabla \otimes \mathbf{v} + \left(\nabla \otimes \mathbf{v}\right)^{\mathrm{T}}\right) \tag{2}$$

In Eq. 1,2 ρ is a density, $\mathbf{v}$ is a velocity, $\boldsymbol{\sigma}$ is the stress tensor, c_p is a speed of longitudinal waves (P-waves), and c_s is a speed of transverse waves (S-waves). The arising damaged areas (cracks) are taken into account through the use of von Mises criterion[22].

The three different problem definitions are considered. The first one is defined by the size of the region of integration 7×7 km^2. In the second one and third one, the size of region of integration was 9×7 km^2. On the ground surface, the condition of the free boundary is used. Also the non-reflective boundary conditions are used on the sides of the region of integration. The earthquake in all of the cases was located at a depth of 3 km along the OY axis and centrally on the horizontal OX axis. In all of these problem definitions, the ground with the following elastic properties is considered: the speed of longitudinal waves was equal to 4500 m/s, the speed of transverse waves was equal to 2250 m/s, and density was equal to 2500 kg/m^3. The concrete with the following elastic properties is considered: the speed of longitudinal waves was equal to 3650 m/s, the speed of transverse waves was equal to 1825 m/s, and density was equal to 2300 kg/m^3. The time interval was equal to 10^{-5} s in all of the three problem defections. 150 000 time steps were calculated in the case of the first and the second problem definitions. 200 000 time steps were calculated in the case of the third problem definition.

In the first problem definition, the surface buildings were placed directly in the epicenter of the earthquake. In the second problem defection, the building was placed in the 1 km to the right side of the earthquake epicenter. The living buildings with a base of 12 m, ceiling height of 3 m, and the foundation depth of 3 m are considered. The maximum principal stress σ_{MAX} in the concrete appearing in von Mises criteria[22] was equal to 1 MPa. Into the ground around the building, the system of six nested hierarchical grids shown in Fig. 1 was set. In the largest grid space step was equal to 4 m, in the smallest grid space step was equal to 0.0625 m. In the neighboring grids space steps were differed by 2 times.

In the third problem definition the underground facilities were considered. The underground facilities were buried at a distance of 600 m, and remote on 1 km to the right side of the earthquake epicenter. σ_{MAX} being was equal to 1 MPa, 2 MPa, and 5 MPa. Inside the underground facilities there is free boundary condition with imaginary points allowing to carry out the method of calculation inside the region of integration for the points placed at the boundary.

Around the underground facilities, the system of 6 nested hierarchical grids is used. One can find the detailed description of the grid-characteristic method in[14-21].

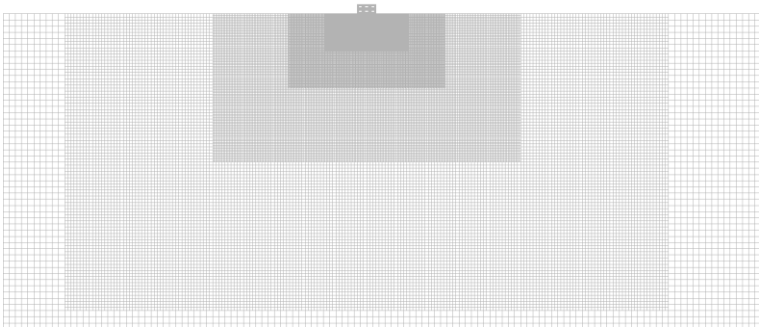

Fig. 1. The system of nested hierarchical grids.

3. The boundary conditions with imaginary points

The boundary conditions with imaginary points for the transport equation, as well as for the case of setting of the Riemann invariant values at the boundary, are considered in[22]. In this paper, the condition of a predetermined pressure $P(t)$ is used realized using the imaginary points and therefore allows through-calculations within the area that is not included in the region of integration. These through-calculations in some cases allows to simplify the problem definition under consideration or reduce the time needed to perform the calculation on the given hardware. In the case of zero-pressure setting, the free-boundary conditions are obtained.

The following formulas are used to correct the values in the adjusted imaginary points. For the three-dimensional case, the correction is carried out using the following formulas for the OX direction:

$$\mathbf{v}_0 = \mathbf{v}_1 \tag{3}$$

$$\mathbf{v}_{-1} = \mathbf{v}_2 \tag{4}$$

$$\boldsymbol{\sigma}_0 = \begin{bmatrix} -2P(t) - \sigma_1^{11} & -\sigma_1^{12} & -\sigma_1^{13} \\ -\sigma_1^{12} & 0 & 0 \\ -\sigma_1^{13} & 0 & 0 \end{bmatrix} \tag{5}$$

$$\boldsymbol{\sigma}_{-1} = \begin{bmatrix} -2P(t) - \sigma_2^{11} & -\sigma_2^{12} & -\sigma_2^{13} \\ -\sigma_2^{12} & 0 & 0 \\ -\sigma_2^{13} & 0 & 0 \end{bmatrix} \tag{6}$$

For the OY direction, the formulas take the following view:

$$\mathbf{v}_0 = \mathbf{v}_1 \tag{7}$$

$$\mathbf{v}_{-1} = \mathbf{v}_2 \tag{8}$$

$$\boldsymbol{\sigma}_0 = \begin{bmatrix} 0 & -\sigma_1^{12} & 0 \\ -\sigma_1^{12} & -2P(t) - \sigma_1^{22} & -\sigma_1^{23} \\ 0 & -\sigma_1^{23} & 0 \end{bmatrix} \tag{9}$$

$$\boldsymbol{\sigma}_{-1} = \begin{bmatrix} 0 & -\sigma_2^{12} & 0 \\ -\sigma_2^{12} & -2P(t) - \sigma_2^{22} & -\sigma_2^{23} \\ 0 & -\sigma_2^{23} & 0 \end{bmatrix} \tag{10}$$

For the OZ direction the formulas take the following form:

$$\mathbf{v}_0 = \mathbf{v}_1 \tag{11}$$

$$\mathbf{v}_{-1} = \mathbf{v}_2 \tag{12}$$

$$\boldsymbol{\sigma}_0 = \begin{bmatrix} 0 & -\sigma_1^{12} & 0 \\ -\sigma_1^{12} & -2P(t) - \sigma_1^{22} & -\sigma_1^{23} \\ 0 & -\sigma_1^{23} & 0 \end{bmatrix} \tag{13}$$

$$\boldsymbol{\sigma}_{-1} = \begin{bmatrix} 0 & -\sigma_2^{12} & 0 \\ -\sigma_2^{12} & -2P(t) - \sigma_2^{22} & -\sigma_2^{23} \\ 0 & -\sigma_2^{23} & 0 \end{bmatrix} \tag{14}$$

In the formulas (3) - (14), the zero subscript index denotes the first imaginary point, a subscript index minus one denotes a second imaginary point, and subscripts 1 and 2 denotes the first and the second internal points in a direction away from the boundary. Superscripts denote the components of the symmetric stress tensor and indicated for a given pressure at the boundary.

Then the method of calculation for the inner points is carried out (through calculation). Note that the calculated wave processes inside the cube (square) crossed out from the region of integration using the imaginary points' boundary do not affect on the wave processes into the region of integration.

4. Seismic waves propagation from the earthquake hypocenter

The seismic waves' propagation from the hypocenter of the earthquake at 0.3 s is shown in Fig. 2a. One can see the generated P-wave (longitudinal wave) and S-wave (transverse wave).

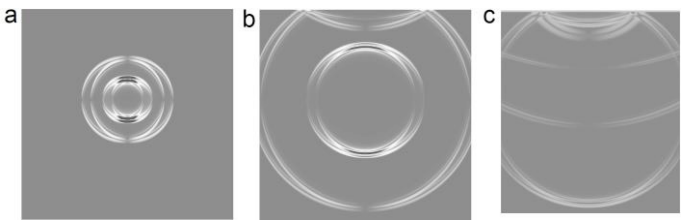

Fig. 2. (a) seismic waves from the hypocenter of the earthquake, time moment 0.3 s; (b) reflection of the P-wave from the Earth surface, time moment 0.8 s; (c) reflection of the S-wave from the Earth surface, time moment 1.5 s.

The wave pattern at 0.8 s is shown in Fig. 2b. The P-wave reflects from the Earth surface and a reflected PP-wave is formed (a longitudinal wave that appears, when the P-wave reflects) and a converted PS-wave (a transverse wave that appears, when the P-wave reflects). And one can see the reflection of the S-wave from the Earth surface at 1.5 s and the formation of the converted SP-wave (the longitudinal wave that appears, when the S-wave reflects) and the reflected SS wave (the transverse wave appears, when the S-wave reflects) in Fig. 2c.

5. The impact on living buildings

One can see that the amplitude of the P-wave directly into the earthquake epicenter is close to zero. As a result in the case of the first problem definition, a whole impact on the ground structure occurs due to the S-wave propagation. The damage that has occurred in the living building as a result of this impact is shown in Fig. 3a.

In the case of the second problem definition, both the P-wave and the S-wave impact on the living building. The impact of the P-wave at 0.69 s is shown in Fig. 4. The damage that has occurred in the living building as a result of this impact is shown in Fig. 3b.

The impact of the S-wave at the 1.43 s is represented in Fig. 5. The total damaged areas in the living building are shown in Fig. 3c.

The gray scale shows the velocity modulus in Fig. 2, 4, 5. It can be seen that, when the living building is located directly into earthquake epicenter, the damaged areas are generally localized symmetrically. In the case of the second problem definition one can see more damaged areas near the side of the living building that is closer to the earthquake epicenter. Also in the case of the second problem definition, it can be seen that the most of the damage occurs as a result of the action of the S-wave.

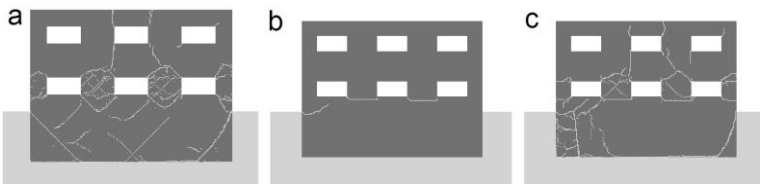

Fig. 3. (a) the damage in the living building, the first problem definition; (b) the damage in the living building due to the P-wave, the second statement; (c) the total damage in the living building, the second statement.

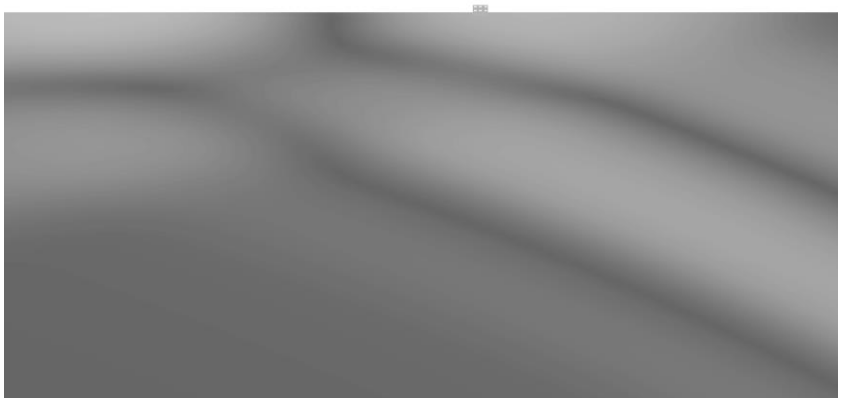

Fig. 4. The impact of the P-wave on the living building. The second statement. The time moment 0.69 s.

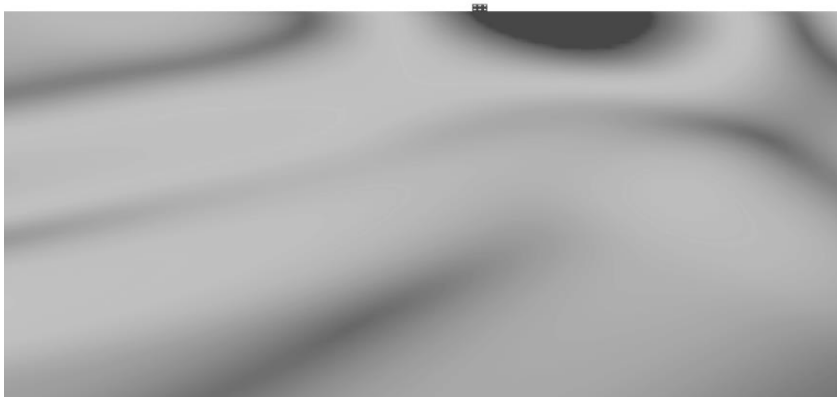

Fig. 5. The impact of the S-wave on the living building. The second statement. The time moment 0.69 s.

6. The impact on underground facilities

The underground facilities are affected by all of 6 types of waves: P-waves, S-waves, reflected PP-waves, converted PS-waves, converted SP-waves, and reflected SS-waves. The impact of the P-wave on the underground facilities at 0.55 s is shown in Fig. 6. The damage resulting from this action for the various maximum stresses that appear in the von Mises criterion[22] is shown in Fig. 7.

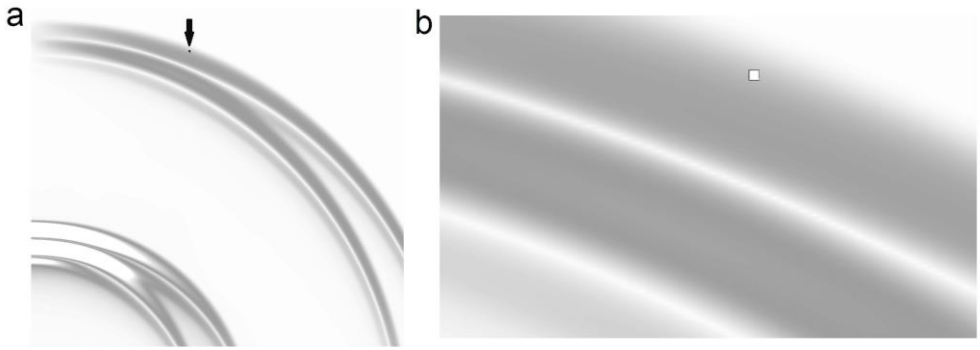

Fig. 6. The impact of the P-wave on the underground facilities. The time moment 0.55 s.

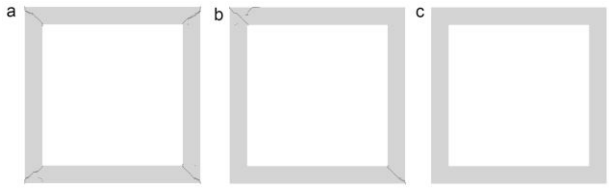

Fig. 7. The damage in the underground facilities due to the P-wave impact for various maximum principal stresses.

The impact of the PS-wave on the underground facilities at 0.98 s is shown in Fig. 8. The damage resulting after this action for the various maximum stresses is shown in Fig. 9.

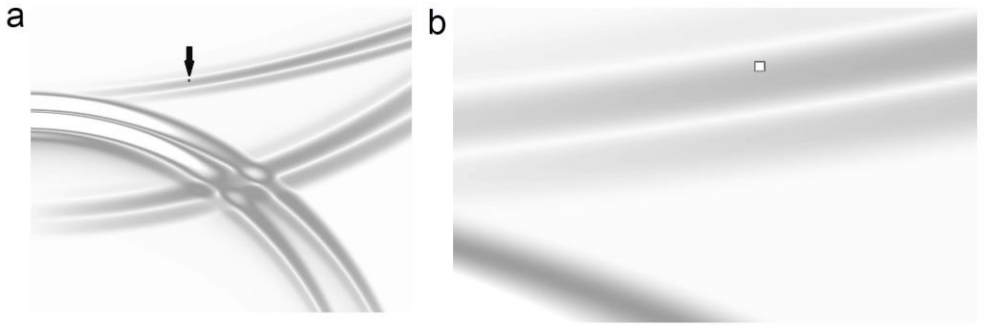

Fig. 8. The impact of the PP-wave on the underground facilities. The time moment 0.98 s.

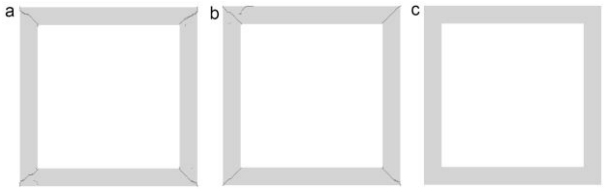

Fig. 9. The damage in the underground facilities due to the P-, PP-, PS-waves impact for various maximum principal stresses.

The impact of the S-wave on the underground facilities at 1.12 s is shown in Fig. 10. The damage resulting after this action for the various maximum stresses is shown in Fig. 11.

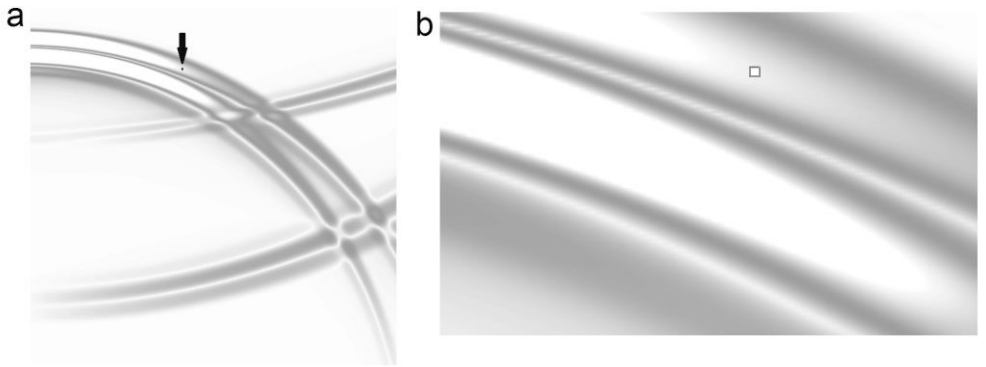

Fig. 10. The impact of the PP-wave on the underground facilities. The time moment 1.12 s.

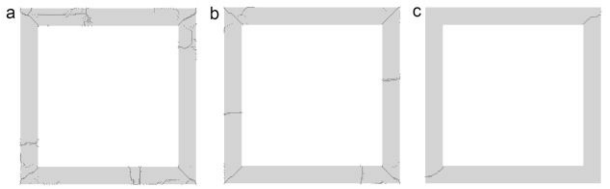

Fig. 11. The damage in the underground facilities due to the P-, PP-, PS-, S-waves impact for various maximum principal stresses.

The impact of the SP-wave on the underground facilities at 1.51 s is shown in Fig. 12. The damage resulting after this action for the various maximum stresses is shown in Fig. 13.

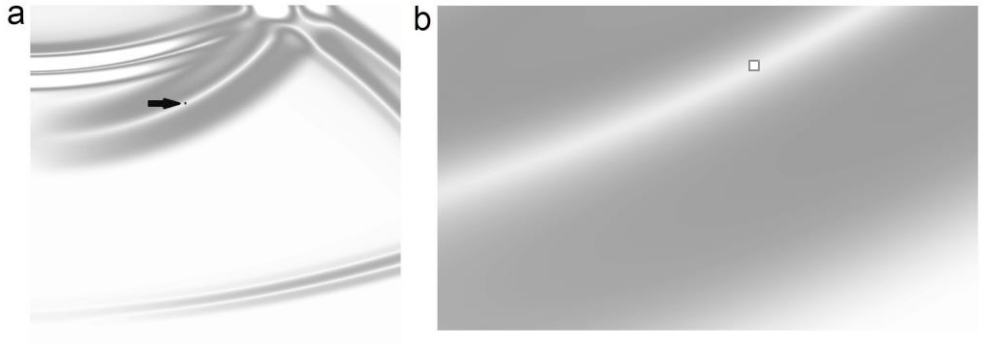

Fig. 12. The impact of the PP-wave on the underground facilities. The time moment 1.51 s.

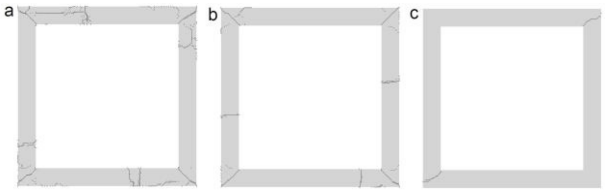

Fig. 13. The damage in the underground facilities due to the P-, PP-, PS-, S-, SP-waves impact for various maximum principal stresses.

The impact of the SS-wave on the underground facilities at 1.67 s is shown in Fig. 14. The total damage for the various maximum stresses is shown in Fig. 15.

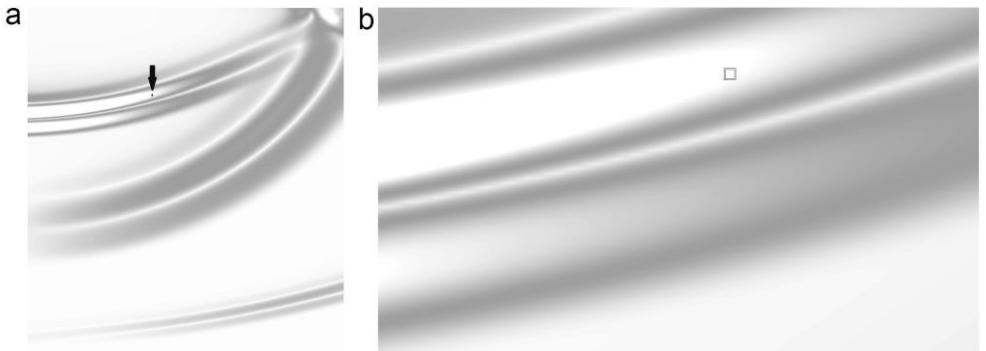

Fig. 14. The impact of the PP-wave on the underground facilities. The time moment 1.67 s.

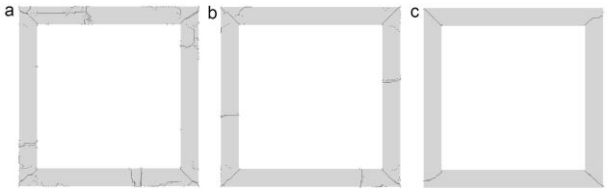

Fig. 15. The total damage in the underground facilities for various maximum principal stresses.

Maximum value of the principal stress was equal to 1 MPa in Fig. 7a, 9a, 11a, 13a, 15a. Maximum value of the principal stress was equal to 2 MPa in Fig. 7b, 9b, 11b, 13b, 15b. Maximum value of the principal stress was equal to 5 MPa in Fig. 7c, 9c, 11c, 13c, 15c. The gray scale shows the velocity modulus in Fig. 6, 8, 10, 12, 14. In Fig. 6b, 8b, 10b, 12b, 14b, while the wave patterns are shown in an enlarged scale as compared to Fig. 6a, 8a, 10a, 12a, 14a.

It can be concluded that the destruction in the underground facilities begins to form at the corners of the structure. The greatest damage occurs when the S-wave is affected, as well as by the reflected SS-wave. The damage due to the impact of the P-wave, and the reflected PP-wave, and the converted PS-wave is not yet observed in the case of 5 MPa maximum value of the principal stress.

7. Conclusions

This paper demonstrates the possibility of numerical modeling the impact of seismic waves propagated from earthquakes' hypocenters to ground buildings and underground facilities located near the surface of the Earth. This possibility is achievable due to the use of systems of nested hierarchical grids around the considered surface and underground structures. Using these nested hierarchical grids can reduce the computational complexity of the task, reduce the amount of Random Access memory (RAM) and the calculation time. The article also demonstrates the advantages of taking into account different types of seismic waves to determine seismic stability of ground and underground objects. This approach allows to analyze the dynamics of the resulting damage and the dependence of the resulting fractures from the types of the impacting seismic waves, the position of the ground or underground structures, the material and construction details of the ground or underground structures.

The arising area of cracks in this ground building (two-storied houses) at different times from different types of seismic waves is studied. Also the impact of earthquake on the underground facilities is considered. A whole impact on the ground structures in earthquakes' epicenters occurs due to the S-wave propagation. The areas of destructions into the underground facilities are caused by all of types of seismic waves: P-waves, S- waves, reflected PP- waves, PS- waves, SP- waves, and SS-waves. The dynamics of arising of areas of destructions into living building and underground structures depends on the material and the design of these structures. And the seismic waves might produce more destructions into the more durable constructions due to the details of the construction.

Acknowledgements

This work was supported by the Russian Science Foundation, grant no. 14-11-00263.

References

1. Madariaga R. Dynamics of an expanding circular fault. *Bull. Seism. Soc. Am.* 1976;**65**;163-182.
2. Virieux J. SH-wave propagation in heterogeneous media: Velocity-stress finite-difference method. *Geophysics* 1984;**49**;1933-1942.
3. Levander AR. Fourth-order finite difference P-SV seismograms. *Geophysics* 1988;**53**;1425-1436.
4. Mora P. Modeling anisotropic seismic waves in 3-D. *59th Ann. Int. Mtg. Exploration Geophysicist, Expanded Articles* 1989;1039-1043.
5. Moczo P, Kristek J, Vavrycuk V, Archuleta RJ, Halada L. 3D heterogeneous staggered-grid finite-difference modeling of seismic motion with volume harmonic and arithmetic averaging of elastic moduli and densities. *Bull. Seism. Soc. Am.* 2002;**92**;3042-3066.

6. Tessmer E. 3-D Seismic modeling of general material anisotropy in the presence of the free surface by Chebyshev spectral method. *Geophysical Journal International* 1995;**59**;464-473.
7. Kaser M, Igel H. A comparative study of explicit differential operators on arbitrary grids. *J. Comput. Acoustics*. 2011;**9**;1111-1125.
8. Carcione JM. The wave equation in generalised coordinates. *Geophysics* 1994;**59**;1911-1919.
9. Tessmer E, Kosloff D. 3-D Elastic modeling with surface topography by a Chebyshev spectral method. *Geophysics* 1994;**59**;464-473.
10. Igel H. Wave propagation in three-dimensional spherical sections by Chebyshev spectral method. *Geophys. J. Int.* 1999;**136**;559-566.
11. Priolo E, Carcione JM, Seriani G. Numerical simulation of interface waves by high-order spectral modeling techniques. *J. acoust. Soc. Am.* 1994;**95**;681-693.
12. Komatitsch D, Vilotte JP. The spectral-element method: an efficient tool to simulate the seismic response of 2D and 3D geological structures. *Bull. Seism. Soc. Am.* 1998;**88**;368-392.
13. Seriani G. 3-D large-scale wave propagation modeling by a spectral-element method on a Cray T3E multiprocessor. *Comput. Methods Appl. Mech. Eng.* 1998;**164**;235-247.
14. Favorskaya A., Petrov I., Khokhlov N. Numerical Modeling of Wave Processes during Shelf Seismic Exploration. *Procedia Computer Science* 2016;**96**;920-929.
15. Petrov I, Vasyukov A, Beklemysheva K, Ermakov A, Favorskaya A. Numerical Modeling of Non-destructive Testing of Composites. Procedia Computer Science 2016;**96**;930-938.
16. Favorskaya AV, Petrov IB. Wave Responses from Oil Reservoirs in the Arctic Shelf Zone. *Doklady Earth Sciences* 2016;**466(2)**;214-217.
17. Petrov IB, Favorskaya AV, Sannikov AV, Kvasov IE. Grid-Characteristic Method Using High Order Interpolation on Tetrahedral Hierarchical Meshes with a Multiple Time Step. *Mathematical Models and Computer Simulations* 2013;**5(5)**;409-415.
18. Golubev VI, Petrov IB, Khokhlov NI. Numerical simulation of seismic activity by the grid-characteristic method. *Computational Mathematics and Mathematical Physics* 2013;**53(10)**;1523-1533.
19. Kvasov IE, Petrov IB. High-performance computer simulation of wave processes in geological media in seismic exploration. *Computational Mathematics and Mathematical Physics* 2012;**52(2)**;302-313
20. Magomedov KM, Kholodov AS. *Grid characteristic methods*. Moscow: Nauka; 1988.
21. Muratov MV, Petrov IB. Estimation of wave responses from subvertical macrofracture systems using a grid characteristic method. *Mathematical Models and Computer Simulations* 2013;**5(5)**;479-491.
22. LeVeque R. *Finite volume methods for hyperbolic problems*. Cambridge University Press; 2002.